# Thermal Airborne Spectrographic Imager for Temperature and Emissivity Retrieval

L. Pipia, F. Pérez, A. Tardà, L. Martínez, V. Pala and R. Arbiol
*Institut Cartogràfic de Catalunya (ICC) Remote Sensing Department, Barcelona, Spain*
{luca.pipia, fernandop,anna.tarda,vicenc.pala,lucas.martinez,arbiol}@icc.cat

*The Thermal Airborne Spectrographic Imager 600 (TASI-600) is a hyperspectral infrared sensor manufactured by the Canadian company ITRES© which started being operated by the Institut Cartogràfic de Catalunya (ICC) at the end of 2009. The system works in a pushbroom configuration and provides the user with 32-band hyperspectral data obtained through a spectral alignment operation in the nominal 8-11.5 µm range. In this work, the effects of spectral interpolation on pixels' radiance balance are shown to yield pixels' absolute temperature uncertainties proportional to emissivity if nominal atmosphere compensation is carried out. Accordingly, an alternative processing chain to cope with this issue is put forward. The estimation of absolute temperature is carried out using ARTEMISS technique* (Borel, 2008). *Results are finally assessed using ground-truth measurements obtained with multiband field radiometers.*

## 1 The TASI Sensor

The Thermal Airborne Spectrographic Imager (TASI) by ITRES© is a pushbroom hyperspectral sensor with a 40º Field-Of-View (FOV) operating in the thermal infrared (TIR) spectral region. It nominally acquires 32 bands to provide continuous spectral coverage in the wavelength range of 8-11.5µm (Itres, 2010). Thermal IR photons emitted from the scene are focused on a plane through two curved slits, generating hyperspectral images with 640 across-track pixels with 6% overlapping.

TASI actually acquires radiance information in 55-bands ranging from 6.5µm up to 12µm approximately. Bands at the shorter wavelengths are employed to estimate pixels' spectral shift induced by temperature variation within airborne platform. Remaining bands are radiometrically calibrated (Radcorr block), spectrally aligned (Specorr block) and filtered in space or frequency by user as needed for blinking pixels removal. At the end of the ITRES traceable processing chain, 32-band hyperspectral data at the system nominal wavelengths are provided.

## 2 Spectral Interpolation Drawbacks

Spectral Interpolation carried out at radiance level might lead to temperature miscalculation due to the difference between nominal and real central wavelength of TASI's filters and, consequently, to an incorrect MODTRAN-based atmospheric contribution removal. This is stressed in the example of Fig. 1, where it can be seen that the transmissivity τ characterizing the interpolated radiance (red filter) from real measurements (blue filters) differs appreciably from the value estimated by MODTRAN5.0 (Berk A. at al.. 2005).

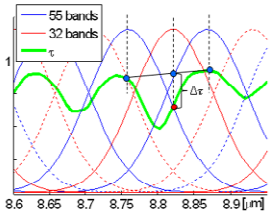


Fig.1: Incorrect atmospheric compensation due to radiance spectral interpolation.

Accordingly, an atmospheric compensation based on the nominal position of sensor's bands might turn out to incorrect. The error in terms of temperature is proportional to scene's emissivity itself, in a way that, the lower the emissivity, the higher the temperature uncertainty. This is shown in Fig. 2 for emissivity ε values spanning within the [0.2, 0.7] interval.

## 3 TASI Processing Chain

A novel processing chain was developed by ICC for an accurate retrieval of absolute temperature and emissivity information from TASI acquisitions. Hyperspectral energy is sampled by TASI at a fixed frequency equal to 200 Hz. Energy frames are then grouped and time-normalized in order to provide squared-pixel radiance information. A first radiometric calibration is carried out using the ITRES© procedure.

An additional calibration block called *RadCapp* developed by ICC is then applied. Essentially, calibration polynomials are used in a pixel-by-pixel approach to make up for hyperspectral radiance systematic underestimation caused by calibration blackbody emissivity uncertainties (Quatrocchi, 2000).

Afterwards, the problem of atmosphere contribution is tackled. Geometrical parameters characterizing each pixel are first estimated.

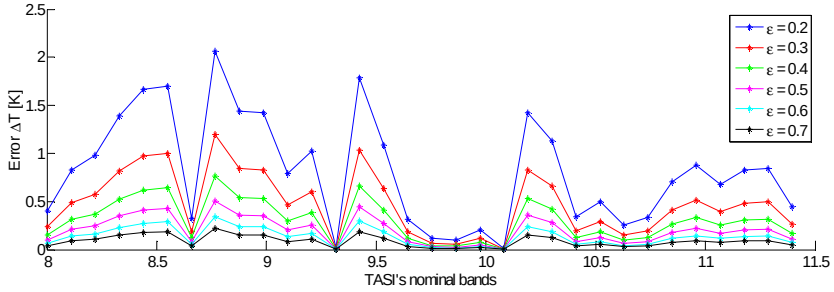


Fig. 2 : Absolute temperature error due to radiance spectral interpolation for ε spanning from 0.2 to 0.7.

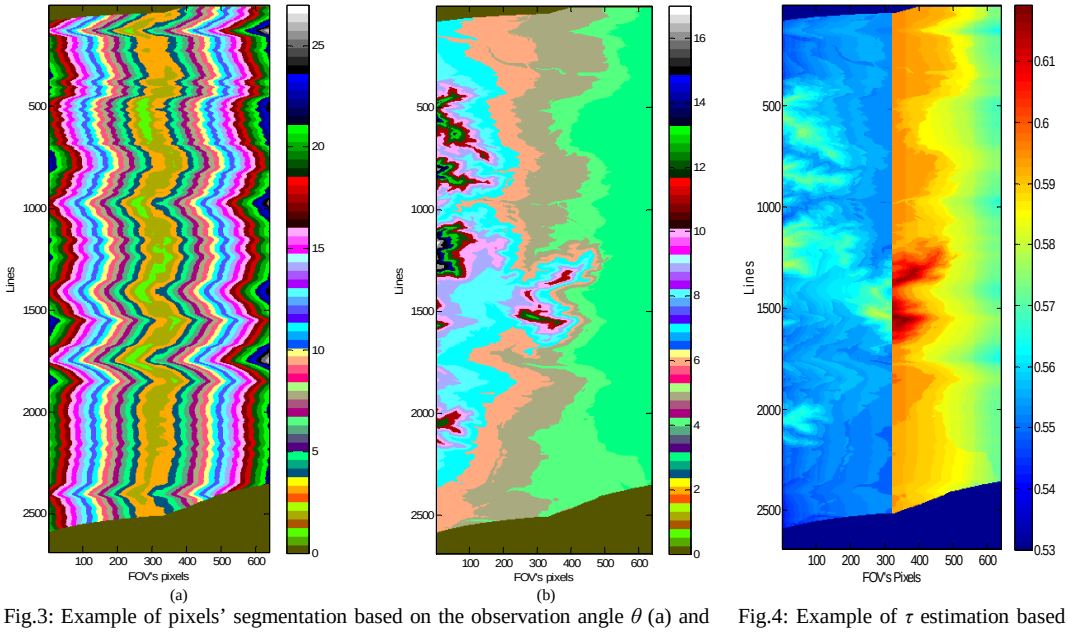


(a) (b)

Fig.3: Example of pixels' segmentation based on the observation angle $\theta$ (a) and vertical distance to the sensor $h$ (b) with $\Delta\theta$=1.5º and $\Delta h$=30m (Vandellós).

Fig.4: Example of $\tau$ estimation based on segmentation of Fig. 3a-b (Vandellós).

Denoting with $l$ and $p$ the image line and FOV's pixel indices, the observation angle $\theta(l,p)$ and the vertical distance to the sensor $h(l,p)$ are calculated for each point of the hyperspectral image in the sensor reference system. Then, height minimum increment $\Delta h$ and angular step $\Delta\theta$ are fixed to group pixels into subsets, as it is shown in Fig. 3a and Fig. 3b. The number of angular sectors and height intervals are equal to

$$N_\theta = \theta_{max}/\Delta\theta \quad (1)$$

$$N_h = h_{max}/\Delta h \quad (2)$$

where $\theta_{max}$ is fixed to 30º (>FOV/2) to take into account turbulence effects.

At this point, MODTRAN5.0 (Berk A. et al, 2005) is employed to estimate atmospheric down-welling radiance $L^{\downarrow}(\lambda)$, upwelling radiance $L^{\uparrow}(\lambda)$ and transmissivity $\tau(\lambda)$ profiles for the $N_\theta \times N_h$ possible geometries in the [6µm,12µm] spectral range. Note that a wavelength range wider than the nominal [8µm, 11.5µm] span is required to deal with possible spectral shifts of the 55 bands actually acquired by TASI.

The last step is to match the spectral properties of FOV's pixels to the corresponding observation geometry, which slightly changes at each line of the hyperspectral image. The hyperspectral filter $f$ imaging pixel $p$ of the FOV in a specific band $b$ is Gaussian-shaped. Then, it is fully-characterized by the central wavelength $\lambda_0(p)$ and the spectral bandwidth $\Delta\lambda(p)$ and can be expressed as

$$f(p,b)=G(\lambda 0(p),\Delta\lambda(p)). \quad (3)$$

where $G$ stands for the normalized Gaussian function.

It follows that the three atmospheric contributions affecting the radiance information provided by pixel $p$ of TASI images at line $l$ in the band $b$ can be modeled as

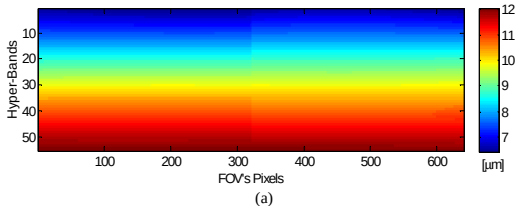

(a)

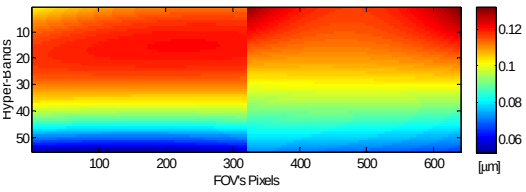

(b)

Fig. 5: Example of the distribution of central wavelength $\lambda_0$ (a) and bandwidth $\Delta\lambda$ (b) of FOV's pixels among the 55 bands acquired by TASI.

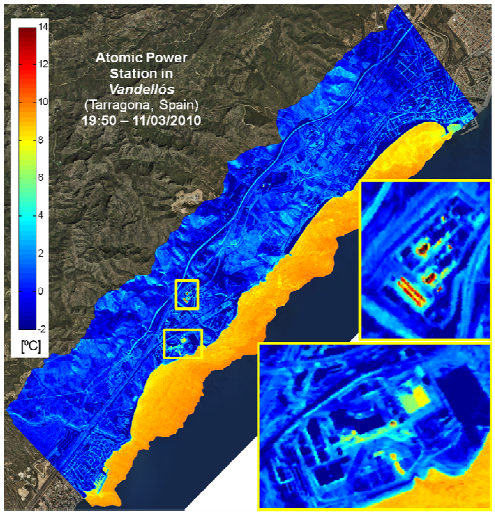


Fig.6: Temperature map of Vandellós retrieved from TASI hyperspectral data using MODTRAN5.0 atmosphere standard model and ARTEMISS technique.

$$\underline{L}^{\downarrow}(l,p,b)=L^{\downarrow}([\frac{\theta(l,p)}{\Delta\theta}],[\frac{h(l,p)}{\Delta h}],b)\cdot G(\lambda_0(p,b),\Delta\lambda(p,b))$$
$$\underline{L}^{\uparrow}(l,p,b)=L^{\uparrow}([\frac{\theta(l,p)}{\Delta\theta}],[\frac{h(l,p)}{\Delta h}],b)\cdot G(\lambda_0(p,b),\Delta\lambda(p,b))$$
$$\underline{\tau}(l,p,b)=\tau([\frac{\theta(l,p)}{\Delta\theta}],[\frac{h(l,p)}{\Delta h}],b)\cdot G(\lambda_0(p,b),\Delta\lambda(p,b)) \quad (4)$$

where [..] denotes the floor function and defines the subset pixel $p$ at the specific line $l$ belongs to. Fig.4 shows an example of the spatial distribution the transmissivity $\tau$ corresponding to a TASI acquisition in Vandellòs (south Catalonia) when $b$=25. Note that differences in filters' spectral properties as well as in pixels' observation geometry turn into changes in the estimation of the atmospheric attenuation to be compensated for. The discontinuity between left and right halves of $\tau$ in Fig.4 is due to spectral differences between the two slits imaging the incoming radiance. This is shown in Fig.5a and Fig. 5b, where an example of the distribution of $\lambda_0(p)$ and $\Delta\lambda(p)$ among the 55 bands acquired by TASI is given.

The last step of the processing chain is the separation of emissivity $\varepsilon(\lambda)$ and temperature $T$ information. Among the alternative techniques available in the literature (Borel, 2008) (Borel, 2003) (Gillespie, 1998), the *Automatic Retrieval of Temperature and EMIssivity* using *Spectral Smoothness* (ARTEMISS) algorithm is used.

In contrast to the first version of the ARTEMISS technique proposed in (Borel, 2003), which essentially finds $T_{opt}$ by maximizing the smoothness of emissivity profile $\varepsilon(b)$, the radiance fitting-based approach described in (Borel, 2008) is more suitable for TASI acquisitions. According to simulations, this minimization approach needs a lower number of hyperspectral bands to converge to the correct temperature information. Then, it better deals with the 32-band data provided by TASI for quantitative parameters estimation.

It is acknowledged that $\varepsilon(\lambda)$ and $T$ are coupled in the equation describing the radiation measured by a hyperspectral TIR sensor $L^S(\lambda)$, which is generally expressed as

$$L^S(\lambda)= [L^{\downarrow}(\lambda)\,(1-\varepsilon(\lambda))+ \varepsilon(\lambda)B(T,\lambda)]\tau(\lambda)+ L^{\uparrow}(\lambda), \quad (5)$$

where $B$ is the Planck's function. The rationale of ARTEMISS is that thermal-infrared spectra of solids are much smoother than gases'.

By defining a reference emissivity (usually $\varepsilon_{ref}$=0.95), a reference temperature $T_{ref}$ is first obtained at pixel level as

$$T_{ref}(l,p)=$$
$$=B^{-1}\{[(\underline{L}^G(l,p,b_0)-\underline{L}^{\downarrow}(l,p,b_0)\,(1-\varepsilon_{ref})]/\varepsilon_{ref},\lambda_0(p,b_0)\} \quad (7)$$

where $B^{-1}$ is the inverse Planck's function and $b_0$ is a TASI spectral band where atmosphere is highly transmissive. Then, $T_{ref}$ is used as input seed to an iterative function fitting the measured and estimated radiances. The optimum temperature is finally given, pixel-by-pixel, by

$$T_{opt}=\min[\sigma\{L^S(l,p,b)-\underline{L}^S(l,p,b,T_{opt},\underline{\varepsilon}_{opt})\}] \quad (8)$$

where

$$\underline{L}^S(\ldots)=[\underline{L}^{\downarrow}(l,p,b)(1-\underline{\varepsilon}_{opt}(b))-\underline{\varepsilon}_{opt}(b)B(T_{opt},b)]\cdot$$
$$\cdot\underline{\tau}(l,p,b)+\underline{L}^{\uparrow}(l,p,b)\}], \quad (9)$$

and $\underline{\varepsilon}_{opt}$ is the low-pass filtered emissivity profile calculated from $T_{opt}$.

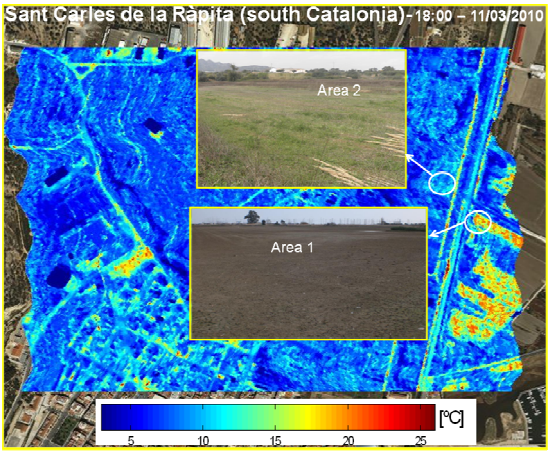


Fig. 6: Temperature map estimated from TASI data of the area close to Sant Carles de la Ràpita.

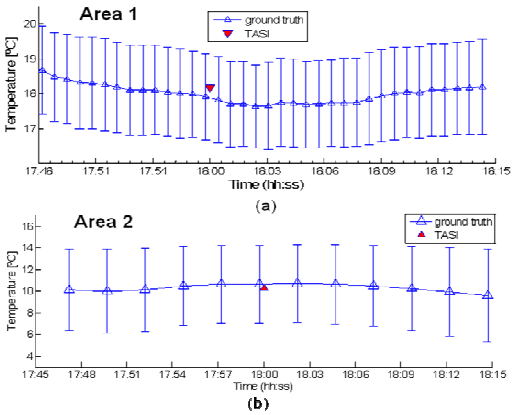


Fig.7: Time evolution of in-situ mean temperature and standard deviation versus TASI estimation concerning the bare soil (a) and low-vegetated (b) areas selected for TASI assessment.

## 4 TASI Real Measurements

First flights with TASI sensor were carried out by ICC in the areas of Vandellòs and Ebre delta, in south Catalonia (Spain). Datasets were acquired on 11/03/2010 at two different heights - 1600m and 3200m- providing images with a pixel size about 2m×2m and 4m×4m, respectively. For the estimation of the atmospheric parameters in the TIR region, the mid-latitude winter model was used. Hyperspectral data were processed as explained in Section 2. The geocoded temperature map retrieved by ARTEMISS for the area of Vandellòs is shown as an example in Fig. 5. The two zoomed subareas correspond to the facilities of a power station over which the TASI sensor was flown.

In order to perform a first assessment of TASI hyperspectral acquisitions, in-situ measurements were also carried out in the framework of a collaboration between the Institut Cartogràfic de Catalunya (ICC) and the Universitat de València Estudi General (UVEG). For this purpose, two test-areas were selected close to Sant Carles de la Ràpita village, one corresponding to bare soil and another one to meadows. In-situ measurements were acquired during TASI passage using two multiband field radiometers, CIMEL CE 312-1 and CIMEL CE312-2. Absolute ground temperature information was obtained by averaging the values retrieved by inverting the Planck's equation from each band with the emissivity values given by the TES technique (Gillespie, 1998). The temperature map estimated from TASI data over the test-areas is shown in Fig. 6 whereas the time-evolution of in-situ temperature mean-value and standard deviation is displayed in Figs. 7a and 7b, respectively.

In order to match TASI and in-situ measurements, a 5×5 boxcar around UVEG field-GPS coordinates was used to average the temperature retrieved by TASI data. The outcome is represented by the red triangle in Fig. 7a and Fig7b. It can be observed a very good matching between the TASI-based and in-situ temperature information, with an error of 0.4K and 0.3K for bare soil and low-vegetation, respectively. The results constitute a first assessment of the quality of hyperspectral data acquired by the TASI sensor as well as of the accuracy of the processing chain implemented by ICC for absolute temperature retrieval.

## 5 Conclusions

A novel processing chain for TASI hyperspectral data has been proposed and assessed using ground-truth measurements. Absolute temperature information was retrieved with an error of 0.3K/0.4K using standard atmospheric profile available in MODTRAN5.0 software. In the near future, improvements provided by in-situ radio-sounding will be assessed and comparisons between retrieved and ASTER-based emissivity profiles will be also performed.

## References

Berk A. at al.. 2005, MODTRAN 5: A Reformulated Atmospheric Band Model with Auxiliary Species and Practical Multiple Scattering Options: Update, *Proceedings of the SPIE*, Vol. **5806**, pp. 662-667.

Borel, C. 2003, ARTEMISS-an Algorithm to Retrieve Temperature and Emissivity from Hyper-Spectral

Thermal Image Data, 28th Annual GOMACTTech Conference, Mar. 31-Apr.3, Tampa, Florida.

Borel, C. 2008, Error analysis for a temperature and emissivity retrieval algorithm for hyperspectral imaging data, *International Journal of Remote Sensing*, No. **17**-**18**, Vol. **29**, 239-246.

Gillespie, A.R., S. Rokugawa, T. Matsunaga, J.S. Cothern, S. Hook, and A.B. Kahle, Temperature and Emissivity Separation from Advanced Spaceborne Thermal Emission and Reflection Radiometer (ASTER) images, Transaction of Geoscience and Remote Sensing, Vol. 35, No. 4, 1113-1126.

ITRES 2010, http://www.itres.com/products/imagers/tasi600 .

Quatrocchi D.A. and Luvall J.C., 2000, Thermal Remote Sensing in Land Surface Process (Boca Raton, London, New York, Washington D.C: CRC Press)